Electronic Supplementary Information for

Self-powered image array composed of touch-free sensors fabricated with semiconductor nanowires

Sangmoon Han,[‡ab] Seoung-Ki Lee,[‡c] Jong-Woong Kim,[a] Sukang Bae,[d] Sang-Hoon Bae,[b] Kwang-Hun Choi[d] and Jin Soo Kim*[a]

[a]Department of Electronic and Information Materials Engineering, Division of Advanced Materials Engineering, and Research Center of Advanced Materials Development, Jeonbuk National University, Jeonju 54896, South Korea.

[b]Mechanical Engineering and Materials Science, Washington University in Saint Louis, MO 63130, USA

[c]School of Materials Science and Engineering, Pusan National University, Busan 46241, South Korea.

[d]Functional Composite Materials Research Center, Korea Institute of Science and Technology (KIST), Wanju, 55324, South Korea.

[‡]These authors contributed equally.

*Corresponding author e-mail address: kjinsoo@jbnu.ac.kr (J.S. Kim) Tel.: +82-63-270-2291; Fax: +82-63-270-2305

Characterization of the InN nanowires (NWs) and the self-powered touch-free sensors (TFSs).

For the formation of undoped InN NWs on a Si(111) substrate, a new growth method, *so called* In pre-deposition, was used with a plasma-assisted molecular-beam epitaxy. A field-emission scanning electron microscopy (FE-SEM, installed in the Future Energy Convergence Core Center at Jeonbuk National University), a double crystal x-ray diffraction (XRD) with a model of MAX-2500 (Cu K_{α}), and a transmission electron microscopy (TEM) with a model of Jeol Jem-arm200F were used to investigate the structural properties of the InN NWs.

The open-circuit voltage (OCV) and current of the TFS were measured using a source meter with a model of Keithley 2400. The capacitances were measured using an LCR meter with a model of Instek LCR-6100. The TFS image array (IA) was analyzed using a data acquisition system with a model of NI PXIe-8300 with the 8 channels (NI TB-4300). The data were acquired with the self-powered TFS-IA with an active medium sized 3.2×3.2 cm^2. Because the area occupied by the TFS-IA is smaller than that of the hand, its imaging range was extended by systematically moving the measuring position. Before the measurements, the positions to be measured were marked on the back of the hand. For a certain position, the hand first remained at a distance of 40 cm from the surface of the TFS-IA and then approached the surface until reaching a distance of 5 cm above the surface to allow the corresponding OCV to be measured. The spatial OCV distribution was converted into an image using the MATLAB image-plot system (MathWorks). For each designated point, this measurement process was repeated according to the step sequence. The measurement process was carried out on 16 locations.

Calculation of the dielectric constant of TFS.

The dielectric constant of the InN NWs is simply calculated using the following equation;[1]

$$\varepsilon = (C \times d)/(A \times \varepsilon_o) \quad (1)$$

where the ε is dielectric constant, C is capacitance, d is operating distance, A is the effective area of the TFS, and ε_o is the vacuum permittivity. Given that the capacitance value of the Si substrate according to the operating distance is negligible, we assumed that the capacitance and dielectric constant of the self-powered TFS are mainly originated from InN NWs.

Calculation on the amount of electric charges of surface ($Q_{surface}$) of TFS according to operating distance.

The $Q_{surface}$ is simply calculated using following equation;[2,3]

$$Q_{Surface} = C \times V_{OC} = \varepsilon \frac{\varepsilon_o A}{d} \times V_{OC}$$

where the C is capacitance and V_{OC} is the maximum OCV of the TFS. Considering the time-dependent OCV and capacitance value of the Si substrate, the electrostatic induction at the Si substrate is negligible (refer to Fig. S6 and S7). From this consideration, we assumed that the capacitance and $Q_{surface}$ of the self-powered TFS are mainly originated from InN NWs.

FE-SEM images of InN NWs with different lengths

Fig. S1 shows the cross-sectional FE-SEM images of the InN NWs with the average length of (a) 137.5±9.8, (b) 322.7±10.2, (c) 483.5±12.1, (d) 832.7±12.5, and (e) 1053.8±15.1 nm. The average diameters at the top (bottom) regions of InN NWs were measured to be (a) 35.2±3.8 (23.1±2.2), (b) 35.5±4.1 (23.2±2.5), (c) 37.7±4.8 (23.2±2.4), (d) 37.8±4.5 (23.2±2.4), and (e) 38.1±4.2 nm (23.2±2.6 nm).

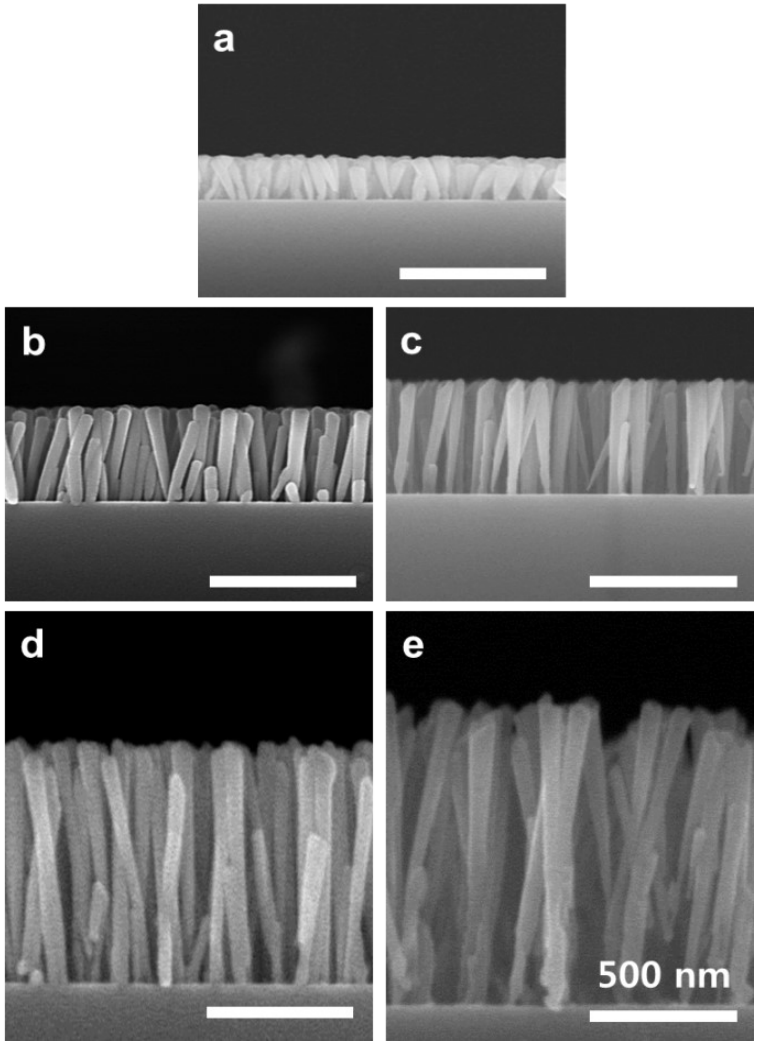

Fig. S1. Cross-sectional FE-SEM images of InN NWs with the average length of (a) 137.5±9.8, (b) 322.7±10.2, (c) 483.5±12.1, (d) 832.7±12.5, and (e) 1053.8±15.1 nm.

OCV curves of TFSs fabricated with InN NWs with different lengths

Fig. S2 shows the time-dependent OCV curves of the TFS fabricated with InN NWs with different lengths. The average OCVs of the InN NWs with the average length of (a) 137.5, (b) 322.7, (c) 483.5, (d) 832.7, and (e) 1053.8 nm were measured to be 0.32±0.04, 0.56±0.08, 0.84±0.06, 0.84 ±0.06, and 0.78±0.02 V. The OCV increases with increasing the length of InN NWs up to 483.5 nm, which is attributed to the increase in $Q_{surface}$ dominantly due to the enlarged active surface area.[1,4] For further increasing the length of the InN NWs above 483.5 nm, the OCV value is saturated and then, slightly decreases due to the increase in the effect of the length of InN NWs on $Q_{surface}$.[3,5]

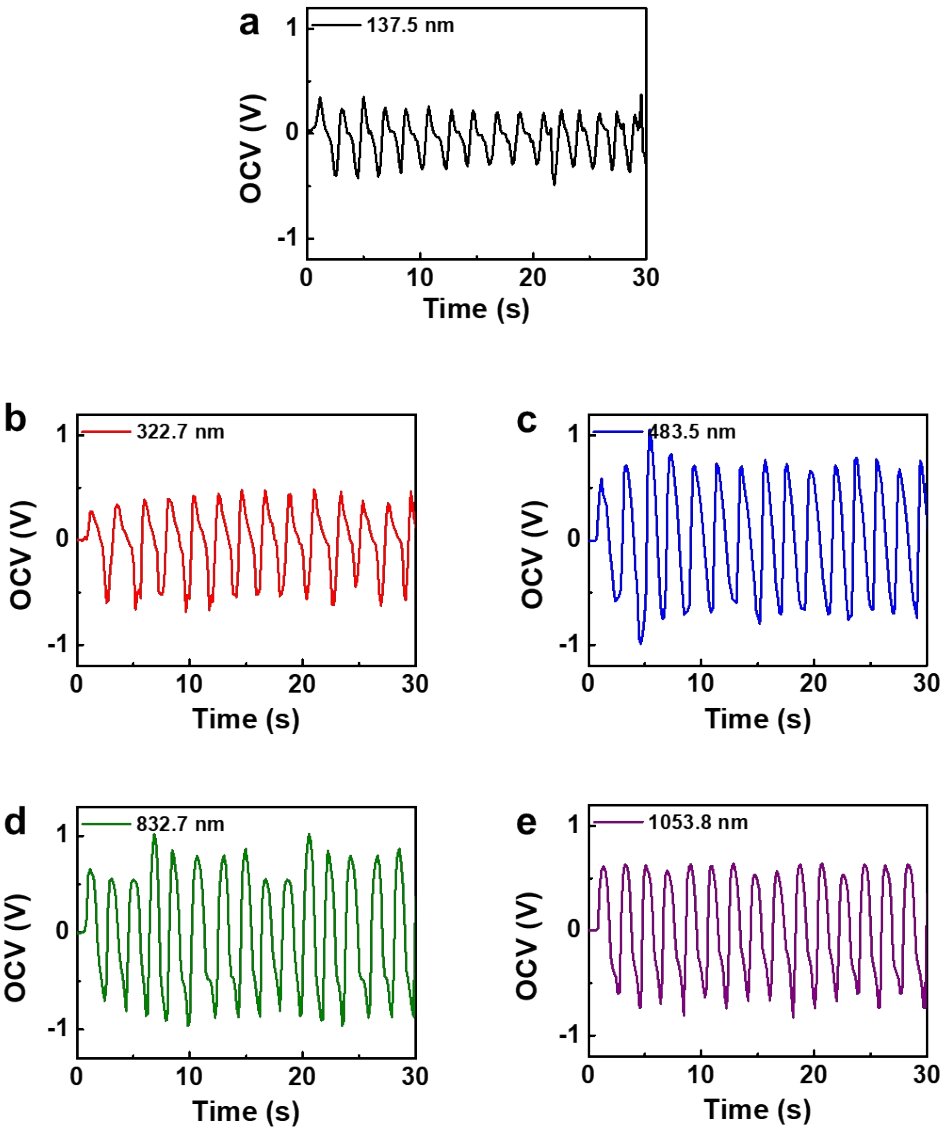

Fig. S2. OCVs of the TFS fabricated with InN NWs with the length of (a) 137.5, (b) 322.7, (c) 483.5, (d) 832.7, and (e) 1053.8 nm.

OCV curves of the TFS according to the number of fingers

Fig. S3 shows the OCV of the TFS while the number of extended human fingers is changed to observe the influence of the effective area of human skin. The OCV was measured to be 0.77±0.09, 0.78±0.08, 0.80±0.09, and 0.81±0.09 V for one, two, three, and four fingers, respectively.

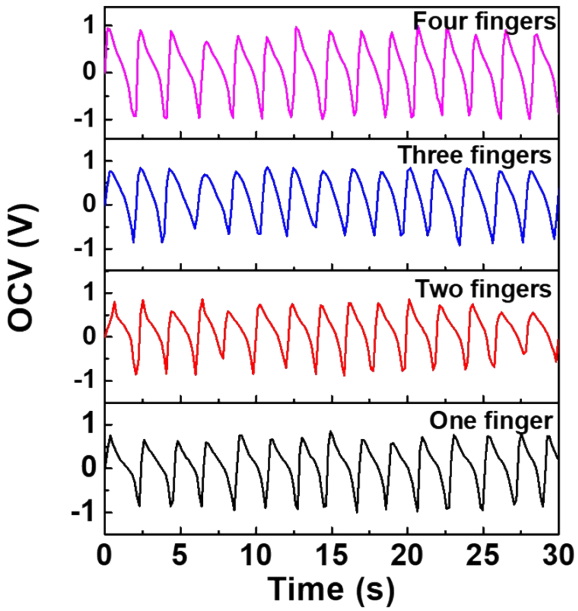

Fig. S3. OCVs of the TFS according to the number of fingers at the operating distance of 1 cm.

OCV curves of the TFS measured immediately, one day, and seven days after the device fabrication

Fig. S4 shows the time-dependent OCV curves of the TFS measured immediately, one day, and seven days after the device fabrication to evaluate the its reliability and stability. The OCV values measured immediately, one day, and seven days after the device fabrication were measured to be 0.84±0.09, 0.84±0.09, and 0.838±0.12 V, respectively.

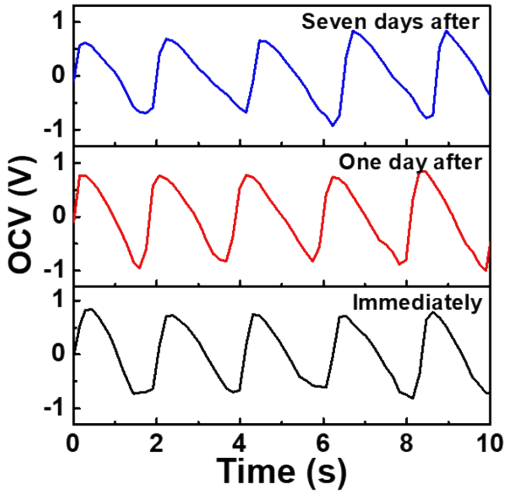

Fig. S4. OCV curves of the TFS measured immediately, one day, and seven days after the device fabrication.

Time-dependent OCV of the TFS according to the various materials.

Fig. S5 shows the time-dependent OCV of the self-powered TFS measured for various materials (polyimide, Al foil, PDMS, polyethylene terephthalate, a sheet of printing paper sized 210 × 297 mm (A4), latex, and polyvinyl chloride) as the sensing materials. The OCVs of the TFS for the polyimide, Al foil, PDMS, PET, A4 sheet, latex, and PVC were measured to be 1.53±0.18, 1.02±0.14, 0.74±0.13, 0.38±0.11, −0.35±0.09, −1.67±0.16, and −8.76±0.24 V, respectively. The change of OCV from positive to negative (from negative to positive) is attributed to the difference in the work function between InN NWs in the TFS and sensing materials.[4]

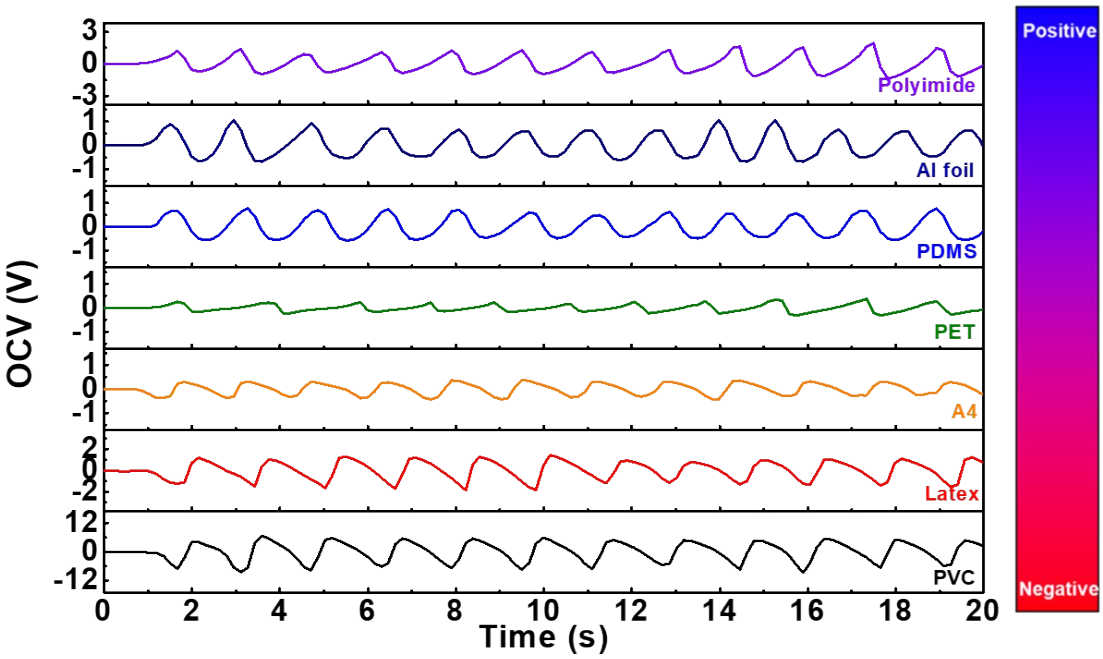

Fig. S5. OCVs of the TFS according to the various materials such as polyimide, Al foil, PDMS, PET, an A4 sheet, latex, and PVC.

Time-dependent OCV of the Si substrate.

Fig. S6 shows the OCV curves of the Si substrate measured at the operating distance of 1 cm, where the motion frequency was fixed as 0.5 Hz. The sample size is 1 x 1 cm^2. To increase electrical conductivity, the Cu electrode was formed on the Pt layer sputtered on the backside of the Si surface. The OCV values were not measured at all time, indicating that the Si substrate is not working as a TFS.

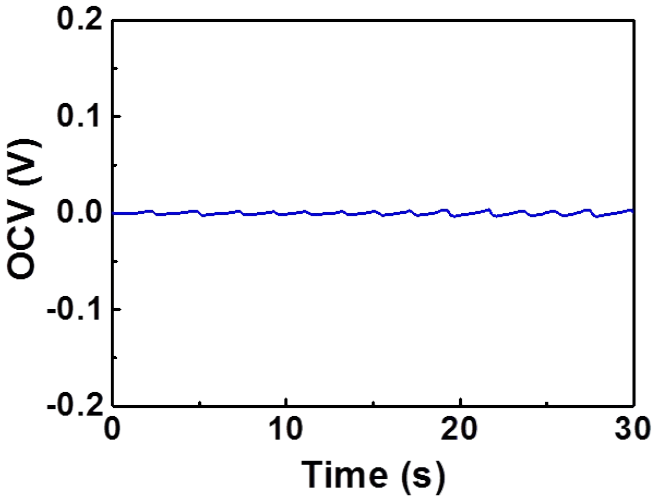

Fig. S6. Time-dependent OCVs of a Si substrate measured at the operating distance of 1 cm.

Summary on the capacitances of the Si substrate.

Fig. S7 shows the summary on the capacitances of a Si substrate with respect to the operating distance, where the motion frequency was fixed as 0.5 Hz. The capacitances were measured immediately after approaching the hand to the substrate. The capacitances at the operating distance of 1, 5, 10, 20, 30, and 40 cm were calculated to be 0.1, 0.1, 0.1, 0.1, 0.1, and 0.05 pF, respectively, which are comparable to noise level.

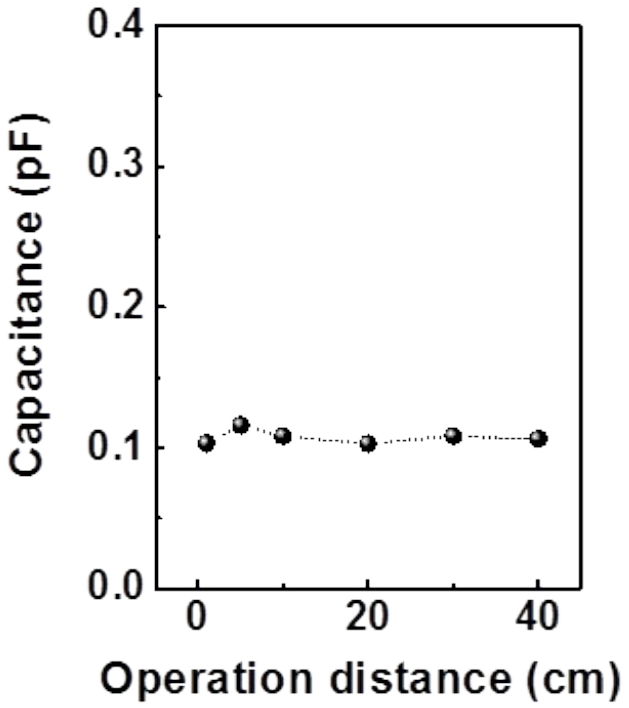

Fig. S7. Summary on the capacitances of a Si substrate measured at various operating distances.

Time-dependent currents of self-powered TFS according to operating distance.

Fig. S8 shows the time-dependent current curves of the TFS measured at different operating distances, where the motion frequency was fixed as 0.5 Hz. The current values at the operating distance of 1, 5, 10, 20, and 30 cm were measured to be 10.2±0.09, 5.6±0.07, 2.6±0.04, 1.3±0.04, and 0.9±0.03 nA, respectively.

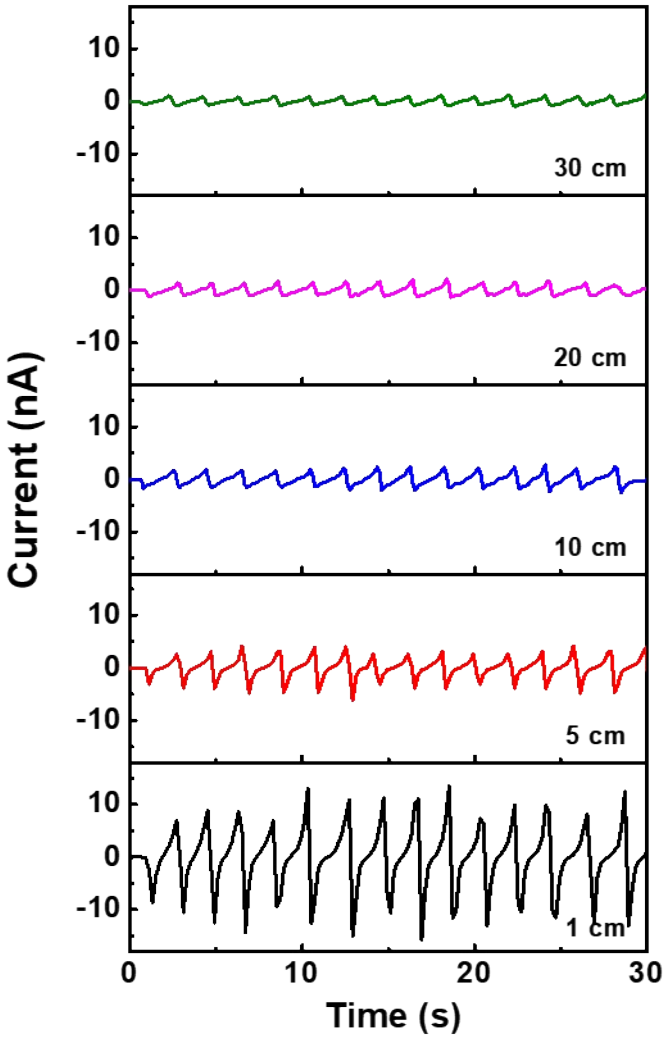

Fig. S8. Time-dependent currents of the TFS according to the operating distance.

$Q_{\text{free-electron}}$ of TFS according to operating distance.

Fig. S9 shows time-dependent $Q_{\text{free-electron}}$ of the TFS measured at the operating distance of 1, 5, 10, 20, and 30 cm, where the motion frequency was fixed as 0.5 Hz. $Q_{\text{free-electron}}$ is simply calculated as the following equation;[6]

$$Q_{free-electron} = \Delta J \times \Delta t$$

where, the ΔJ and Δt are the change in the values of current density and time, respectively.

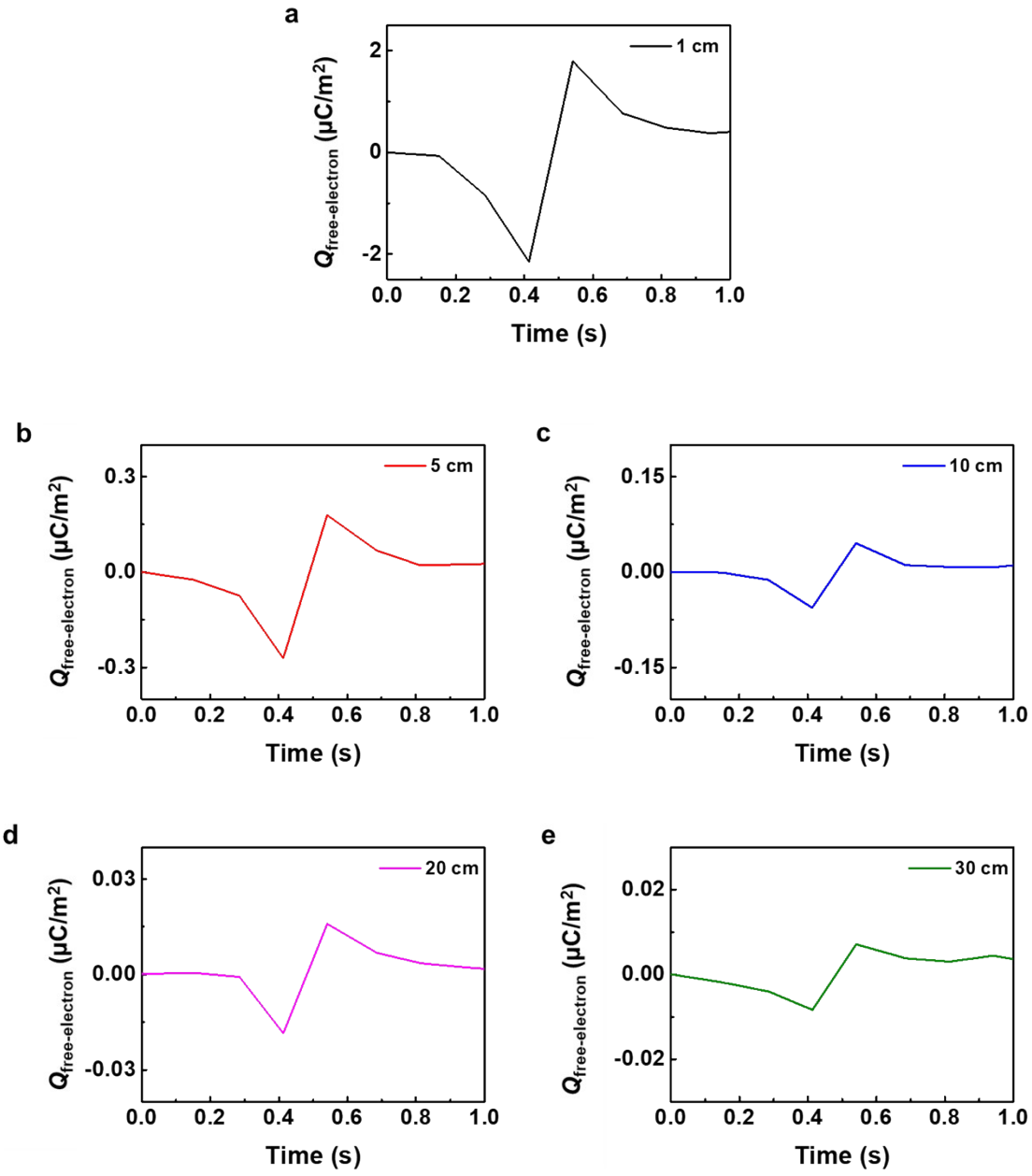

Fig. S9. Time-dependent $Q_{\text{free-electron}}$ of the TFS measured at the operating distance of (a) 1, (b) 5, (c) 10, (d) 20, and (e) 30 cm, where the motion frequency was fixed as 0.5 Hz.

OCVs of TFS according to inter-distances between two neighboring TFSs.

Fig. S10a shows the schematic diagram to evaluate the crosstalk by changing the inter-distance (*d*) between neighboring TFSs (TFS-1 and TFS-2). The distance between TFS-1 and TFS-2 samples was controlled by moving the TFS-2 sample. The OCV of the TFS-1 sample was measured while moving the human hand up and down at a fixed inter-distance (0.1, 0.2, 0.4, and 0.6 cm) between two chips, which are shown in Fig. S10b. The operating distance between the TFS-2 and the human hand was 1 cm. The OCVs at the inter-distance of 0.1, 0.2, 0.4, and 0.6 cm were measured to be 0.83±0.8, 0.35±0.4, 0.21±0.3, and 0.15±0.2 V, respectively. Considering the crosstalk between two TFS samples in our experimental conditions, the inter-distance of 0.4 cm shows the best result among the other distances between two neighboring chips. Therefore, we fabricated the TFS-IA consisting of 16 sensor units with the inter-distance of 0.4 cm.

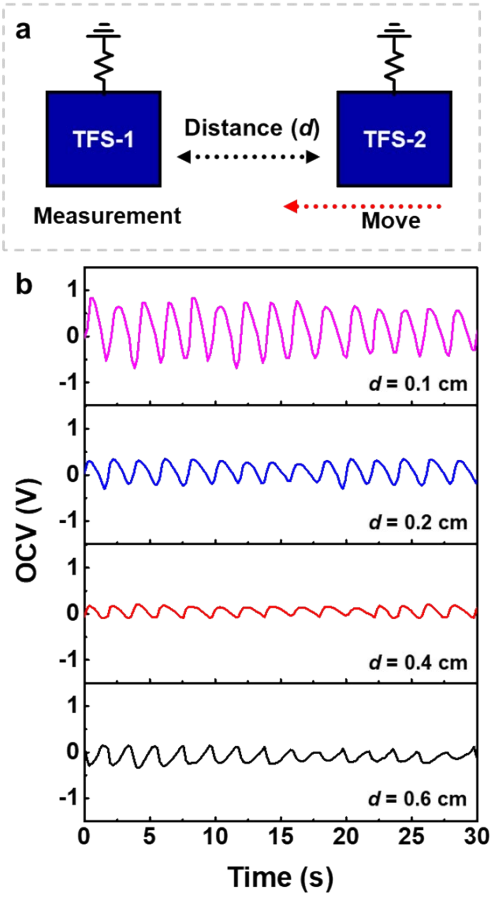

Fig. S10. OCVs for the TFS units according to the inter-distance between two neighboring sensor units.

Measurement of the human hand TFS-IA

The overall size of the TFS-IA is 8 × 8 cm^2, where the total active area is 3.2 × 3.2 cm^2. Because the area occupied by the TFS-IA is smaller than that of the hand, its imaging range was extended by systematically moving the measuring position. Before the measurements, the positions to be measured were marked on the back of the hand. For a certain position, the hand first remained at a distance of 40 cm from the surface of the TFS-IA and then approached the surface until reaching a distance of 5 cm above the surface to allow the corresponding OCV to be measured. The spatial OCV distribution was converted into an image using the MATLAB image-plot system (MathWorks). For each designated point, this measurement process was repeated according to the step sequence. The measurement process was carried out on 16 locations.

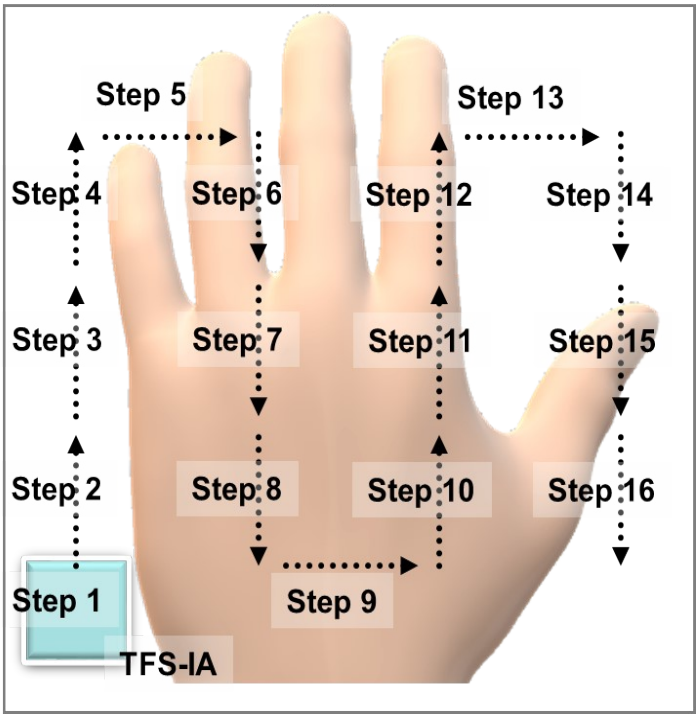

Fig. S11. Measurement method of the backside of a human hand using TFS-IA consisting sixteen TFS units.

References

1. Z. Song, H. Duan, L. Miao, L. Ruhlmann, Y. Lv, W. Xiong, D. Zhu, L. Li, L. Gan and M. Liu, *Carbon* 2020, **168**, 499-507.

2. Y. Zi, J. Wang, S. Wang, S. Li, Z. Wen, H. Guo and Z. L. Wang, *Nat. Commun.* 2016, **7**, 10987.

3. W. Liu, Z. Wang, G. Wang, G. Liu, J. Chen, X. Pu, Y. Xi, X. Wang, H. Guo, C. Hu and Z. L. Wang, *Nat. Commun.* 2019, **10**, 1426.

4. K.-H. Choi, S. Park, S.-K. Hyeong, S. Bae, J.-M. Hong, T.-W. Kim, S. H. Lee, S. Ryu and S.-K. Lee, *J. Mater. Chem. A* 2020, **8**, 19822-19832.

5. S. Niu and Z. L. Wang et al., *Nano Energy* 2015, **14**, 161-192.

6. Y. Tang, H. Zhou, X. Sun, N. Diao, J. Wang, B. Zhang, C. Qin, E. Liang and Y. Mao, *Adv. Funct. Mater.* 2020, **30**, 1907893.